

Article

Lattice Boltzmann Simulation of Ferrofluids Film Boiling

Mohammad Yaghoub Abdollahzadeh Jamalabadi ^{1,2} 

¹ Department for Management of Science and Technology Development, Ton Duc Thang University, Ho Chi Minh City 700000, Vietnam; abdollahzadeh@tdtu.edu.vn

² Faculty of Civil Engineering, Ton Duc Thang University, Ho Chi Minh City 700000, Vietnam

Received: 17 June 2020; Accepted: 16 July 2020; Published: 22 July 2020



Abstract: In the present investigation, two phase film boiling of ferrofluids under an external field delivered around a two-dimensional square cross-section heater was investigated using the lattice Boltzmann technique. The purpose of this work is to find the effect of magnetic field magnitude and direction on the Nusselt number in single and double heater geometry. The improving thermal efficiency in the horizontal and vertical placement of heaters is also presented. The governing equations of mass conservation, momentum conservation, and energy conservation are solved by using a central-moments-based Lattice Boltzmann scheme. The air pocket generated around heater raised incorporating magnetic effects. The heat transfer through this advancement has been explored quantitatively and abstractly. The results shows that with the development in the volumetric applied force at the bubble-fluid interface, the bubble boundary layer thickness around the square heater lessened which cause the Nusselt number augmented. Through the parameter study it found that the Nusselt number can be essentially extended by altering the course of magnet shafts, and that film rising outwardly of the bubble. The improvement and advancement of vapour phase in various heater arrangement made two column of bubble rises at the same time, which rose above each heater and in the end changed into one column of bubble. A correlation considering magnitude and angle of the magnetic field on time-averaged Nusselt number is presented. Finally, the Nusselt number can be controlled with the help of the incorporation of other heaters.

Keywords: numerical simulation; ferrofluids; boiling; Lattice Boltzmann method

1. Introduction

The film boiling heat convection exists in a couple of structuring endeavors and engineering applications, for instance, the cooling of electronic contraptions, microchannel heat exchangers, inert cooling, geothermal science, energy storage in phase change material, sun controlled heat exchangers, and so forth [1–4]. Considering this wide extent of usage, the topic of two-phase flow is engaging for researchers and various assessments have been finished. Since the ordinary heat transfer convection has various applications in the cutting edge of technology, this marvel has been investigated in the applications with different geometries, warm breaking point conditions, power plant working fluid, cooling strategy, and so on [5–9]. Reference [10] performed over the joint effort between the laminar/ordinary convection with surface radiation inside a to a limited extent warmed high perspective extent pit stacked up with air. They declared that the surface radiation has a minor effect on the temperature field and stream structure at the most bits of the pit. Furthermore, the geometrical parameters, for instance, the width and height of the cavity, have a significant impact on the enclosure heat transfer by radiative and convective mode at the lower and upper regions of the cavity. References [11] performed a numerical three-dimensional propagation of natural and forced convection and radiation in a cuboidal isolate zone which is fused by level plates of restricted thickness and with

high and low conductivities. They found that the consistency of the temperature dispersal at the interface redesigns under radiation when the plates with low conductivity are implanted. Additionally, it was exhibited that the convective drop is more diminutive in regions where peak isolate than in those spots where tufts fall on the interfaces. The stormy ordinary and mixed convection in an air-filled alcove with heat source was numerically analyzed by other studies [11,12]. At present, the effects of the geometrical parameters and breaking point conditions of the downturn were presented. Besides, the results got by different k - ϵ aggravation models were presented, broadly. References [12,13] did a couple of assessments using two exploratory courses of action on brutal Rayleigh-Benard trademark convection inside cubical fenced-in territory included with adiabatic side dividers. They exhibited that abstract and quantitative traits of the fluid stream are near disregarding particular differences in the preliminary game plans. What's more, the results demonstrated that quantitative changes of characteristics of a huge extension stream have occurred as Rayleigh number and Prandtl number improve. Reference [14] guided a couple of tests to explore the laminar normal convection in a three-dimensional cuboidal fenced in the region. They finished the examinations for different liquid and Rayleigh numbers. Also, they presented the exploratory results, and the obtained computational data at a comparable plot of the separated region, perspective extents of various liquid, and Rayleigh numbers. They conclude that there is adequate comprehension between the numerical and exploratory results. Reference [15] separated the laminar free convection in an H-formed region with nanofluid. The viscosity and thermal diffusivity of nanofluids have been evaluated by Brookfield viscometer and KD2 properties analyzer, independently. They found that the Rayleigh number increases the Nusselt number. Various examinations have demonstrated that the grid Boltzmann technique is successful in contemplating the convection heat move under different field powers. References [16–29] in constrained convection, results uncovered that temperature inclination decreases with the ascent of Rayleigh number. In normal convection, the normal Nusselt number increments with the expansion of Rayleigh number and the lessening of Hartmann number. Fakhari et al. [21] LBM method for large density and viscosity ratios. LBM compared to MRT, has better accuracy, convergence, and stability. Jamalabadi [22] examined the warmth dispersal impact of ferrofluid regular convection in a slanted depression under the attractive field. Different Rayleigh numbers and slanted edges were considered, and slanted edge at 0 degrees and Rayleigh number at 10^4 ended up being the best circumstance for heat scattering. Jamalabadi [22] additionally examined the warmth dispersal impact of the characteristic convection of a ferrofluid in a cavity with direct temperature conveyance under an attractive field and found that the warm move diminishes by the augmentation of the nanoscale ferromagnetic molecule volume part for different Rayleigh numbers. Jamalabadi [22] recreated the warmth move and entropy age of MHD characteristic convection. Results showed that the expansion in Hartmann's number leads to the warmth move and the absolute entropy age drop. Saito, De Rosi, and Fei [25] explored the fluid constrained convection and common convection heat move improvement under an attractive field utilizing cross-section Boltzmann strategy. A diffuse interface modeling for a three-dimensional problem has been already proposed by Fakhari & Bolster [16], where the multiphase flows are calculated in a three-dimensional model coupled with LBM and diffuse-interface phase-field approaches [26–29]. Krakov and Nikiforov performed studies on the Influence of the uniform outer magnetic field [30] and shape of the inner boundary [31] on thermomagnetic natural convection in a horizontal cylindrical enclosure filled with a magnetic nanofluid. They show that a magnetic field change the convection structure and increase 4–5 times in Nusselt number. Those articles devoted to modeling of thermophysical processes in magnetic fluids.

In this paper, numerical simulation of ferrofluids film boiling by Lattice Boltzmann method is presented. In the next sections, mathematical and numerical modeling are presented. Finally, the effect of magnetic field magnitude and direction on the Nusselt number in single and double heater geometry is presented and discussed.

2. Mathematical Modeling

Figure 1 shows the schematic of the problem. As shown a magnet inside a ferrofluid is confined by free surface of fluid at top and three walls in other direction. The initial vapour is located at the top of the liquid. The mathematical modelling of the problem is specified in following paragraphs which are obtained from Reference [1]. The governing equation of continuity is

$$\nabla \cdot \mathbf{u} = \frac{\dot{q}_f}{h_{fg}} (6 V_f (1 - V_f) \frac{|\nabla \phi|}{2}) \left(\frac{1}{\rho_v} - \frac{1}{\rho_l} \right). \quad (1)$$

As there are many variables in the above equation for explanation of the symbols used in the formula, see the list of parameters in nomenclature. The governing equations of Navier-Stokes are

$$\rho \frac{\partial \mathbf{u}}{\partial t} + \rho (\mathbf{u} \cdot \nabla) \mathbf{u} = \nabla \cdot [-PI + \eta (\nabla \mathbf{u} + \nabla \mathbf{u}^T)] + \rho \mathbf{g} + \left(\lambda \left[-\nabla^2 \phi + \frac{\phi(\phi^2 - 1)}{\varepsilon^2} \right] \right) \nabla \phi - \frac{1}{2} H^2 \nabla \mu. \quad (2)$$

Here, the dependence of the properties of the magnetic fluid and permanent magnets on temperature is ignored, which makes the applicability of this model limited. The form of the magnetic force term in Equation (2) is not general. The governing equation of energy equations is

$$\rho C_p \frac{\partial T}{\partial t} + \rho C_p (\mathbf{u} \cdot \nabla) T = \nabla \cdot k \nabla T - \frac{\dot{q}_f}{h_{fg}} (6 V_f (1 - V_f) \frac{|\nabla \phi|}{2}) h_{fg}. \quad (3)$$

In typical film boiling system considered the fluid temperature is initially near saturation temperature and after phase change it leaves the heater boundary. Because of nature of phase change the system remains near the saturation temperature. Dimensionless temperature ratio, $\frac{T - T_{sat}}{T_w - T_{sat}}$ is near zero. But for finding precise effect of temperature on the system properties further investigations are recommended. The dimensionless number that is important in film boiling is the Jackop number which defined as

$$Ja = c_{p,l} (T_w - T_{sat}) / h_{fg}. \quad (4)$$

The governing equations of Cahn-Hilliard are

$$\frac{\partial \phi}{\partial t} + \mathbf{u} \cdot \nabla \phi - \frac{\dot{q}_f}{h_{fg}} (6 V_f (1 - V_f) \frac{|\nabla \phi|}{2}) \left(\frac{V_{f,v}}{\rho_v} + \frac{V_{f,l}}{\rho_l} \right) = \nabla \cdot \frac{\gamma \lambda}{\varepsilon^2} \nabla \psi, \quad (5)$$

and

$$\psi = -\nabla \cdot \varepsilon^2 \nabla \phi + (\phi^2 - 1) \phi. \quad (6)$$

The physical properties of the system are given in Table 1. The physical properties shown in Table 1 are designed to reach stability in numerical solution. As the nature of film boiling is unsteady process it could be easily transit to the turbulence regime (for $\delta \frac{\sqrt{\tau_w / \rho_v}}{v_v} > 10$) which is out of scope of current research. The aim of the current study is developing a laminar solution for film boiling process.

The governing equation of Amper law are

$$\nabla \times \mathbf{H} = 0, \quad (7)$$

$$\nabla \cdot \mathbf{B} = 0, \quad (8)$$

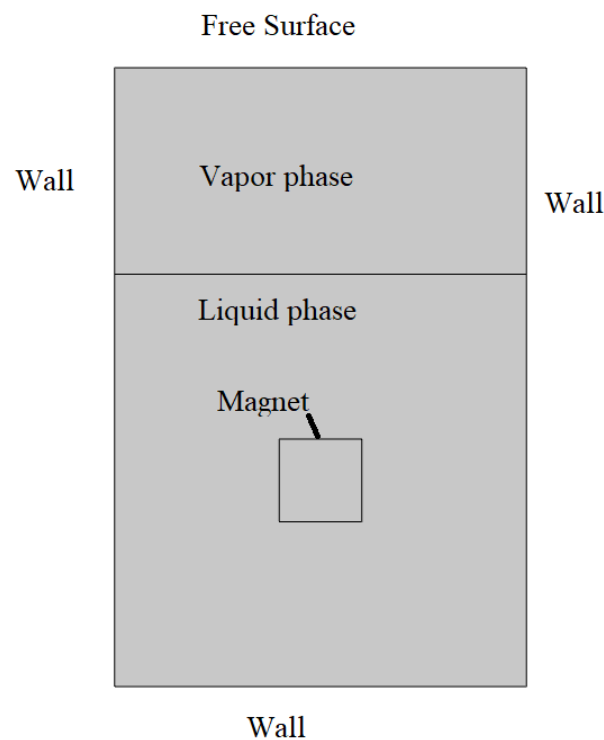
where

$$\mathbf{B} = \mu_0 (1 + \chi) \mathbf{H} = \mu_0 \mu_r \mathbf{H} = \mu \mathbf{H}. \quad (9)$$

Table 1. Physical properties [1].

	Unit	Liquid	Vapour	Magnetic Nanoparticle
Density	kg/m ³	200	5	5600
Thermal conductivity	$\frac{W}{mK}$	40	1	6
Heat capacity	$\frac{J}{kgK}$	400	200	670
Dynamic viscosity	Pa s	0.1	0.005	–
Surface tension	N/m	0.1	–	–
Magnetic susceptibility	1	0.2	0	–
Latent heat	J/kg	10,000	–	–
Volume concentration	1	0.004	–	–

The fundamental boundary condition of vapour gurgling is delineated in Figure 1. As showed up this moment, thin-film is believed to have complied with the warmed heater. The top bit of the region is allocated as the vapour stage to which vapour rises over the long haul. The breaking point applied for disentangling the Maxwell, Navier-Stokes, and imperativeness conditions are delineated underneath.

**Figure 1.** Schematic of the problem.

The boundary condition of velocity at sides

$$u = 0, \quad \frac{\partial v}{\partial x} = 0, \quad (10)$$

$$\frac{\partial T}{\partial x} = 0, \quad (11)$$

and

$$\frac{\partial H}{\partial x} = \frac{\partial H}{\partial y} = 0. \quad (12)$$

The top boundary condition is

$$\frac{\partial u}{\partial y} = \frac{\partial v}{\partial y} = \frac{\partial T}{\partial y} = 0. \quad (13)$$

The boundary condition at the bottom

$$u = v = 0, \quad (14)$$

and

$$\frac{\partial T}{\partial y} = 0. \quad (15)$$

The boundary condition at the heater

$$u = v = 0, \quad (16)$$

$$-k \frac{\partial T}{\partial n} = q_{wall}. \quad (17)$$

As well on the heater, the Nusselt Number is defined as

$$Nu(\theta, t) = \frac{q_{wall} D}{k} \frac{1}{T_w - T_{sat}}, \quad (18)$$

and Nusselt Number in average on angle

$$Nu(t) = \frac{1}{2\pi} \int_0^{2\pi} Nu(\theta, t) d\theta, \quad (19)$$

and Nusselt Number in average on time

$$Nu = \frac{1}{\Delta t} \int_{t_i}^{t_e} Nu(t) dt. \quad (20)$$

3. Numerical Modeling

The method of central moments by the use of local fluid velocity moves the lattice directions. The cross-section Boltzmann technique is a liquid numerical reenactment strategy created throughout the previous thirty years. Applied in numerous zones, which might be hard for customary strategies, for example, small scope stream and warmth move, permeable media, attractive liquid, and so forth. The cross-section Boltzmann technique has the benefits of natural parallelism, just as straightforward limit condition preparing and simple usage of the program.

By the definition of directions (see Figure 2)

$$e_x = [0, 1, -1, 0, 0, 1, -1, 1, -1]^T, \quad (21)$$

$$e_y = [0, 0, 0, 1, -1, 1, -1, -1, 1]^T. \quad (22)$$

The fluid density is

$$\rho = \sum_i f_i, \quad (23)$$

and velocity vector is

$$\rho \mathbf{u} = \sum_i f_i \mathbf{e}_i + \frac{\mathbf{F}}{2} \delta_t. \quad (24)$$

The lattice Boltzmann equation is

$$\frac{Df_\alpha}{Dt} = -\frac{1}{\lambda} (f_\alpha - f_\alpha^{eq}) + \frac{1}{c_s^2} (e_\alpha - u) \cdot F \Gamma_\alpha, \quad (25)$$

where the equilibrium population is

$$f_{\alpha}^{eq} = w_{\alpha} \rho \left[1 + \frac{e_{\alpha} \cdot u}{c_s^2} + \frac{(e_{\alpha} \cdot u)^2}{2c_s^4} - \frac{(u \cdot u)}{2c_s^2} \right], \quad (26)$$

and

$$g_{\alpha} = f_{\alpha} c_s^2 + (p_1 - \rho c_s^2) \Gamma_{\alpha}(0), \quad (27)$$

which

$$g_{\alpha}^{eq} = w_{\alpha} \left[p + \rho c_s^2 \left(\frac{e_{\alpha} \cdot u}{c_s^2} + \frac{(e_{\alpha} \cdot u)^2}{2c_s^4} - \frac{(u \cdot u)}{2c_s^2} \right) \right], \quad (28)$$

and the energy equation

$$\frac{\partial g_{\alpha}}{\partial t} + e_{\alpha} \cdot \nabla g_{\alpha} = -\frac{1}{\lambda} (g_{\alpha} - g_{\alpha}^{eq}) + (e_{\alpha} - u) \cdot [\nabla \rho c_s^2 (\Gamma_{\alpha} - \Gamma_{\alpha}(0)) - C \nabla \mu \Gamma_{\alpha}] + \rho c_s^2 \dot{m}''' \left(\frac{1}{\rho_v} - \frac{1}{\rho_l} \right) \Gamma_{\alpha}(0), \quad (29)$$

while

$$\frac{\partial h_{\alpha}}{\partial t} + e_{\alpha} \cdot \nabla h_{\alpha} = -\frac{1}{\lambda} (h_{\alpha} - h_{\alpha}^{eq}) + (e_{\alpha} - u) \times \left[\nabla C - \frac{C}{\rho c_s^2} (\nabla p + C \nabla \mu) \right] \Gamma_{\alpha} + (M \nabla^2 \mu - \frac{\dot{m}''' \rho_l}{\rho c_s^2}) \Gamma_{\alpha}. \quad (30)$$

The matrix form of evaluation is

$$f_{\alpha}^*(\mathbf{x}, t) = f_{\alpha}(\mathbf{x}, t) - (\mathbf{M}^{-1} \mathbf{\Lambda} \mathbf{M})_{\alpha\beta} (f_{\beta} - f_{\beta}^{eq}) + \Delta t F_{\alpha}'. \quad (31)$$

By a suitable basis of moments [29] and pre-collision central moments [27], the collision operator in terms of central moments is obtained. The matrix M transforms the distribution functions into the raw moments and lower-triangular matrix N shift transform matrix the raw moments into the central moments.

The transformation matrix M is calculated from

$$M = \begin{bmatrix} 1 & 1 & 1 & 1 & 1 & 1 & 1 & 1 & 1 \\ 0 & 1 & -1 & 0 & 0 & 1 & -1 & 1 & -1 \\ 0 & 0 & 0 & 1 & -1 & 1 & -1 & -1 & 1 \\ 0 & 1 & 1 & 1 & 1 & 2 & 2 & 2 & 2 \\ 0 & 1 & 1 & -1 & -1 & 0 & 0 & 0 & 0 \\ 0 & 0 & 0 & 0 & 0 & 1 & 1 & -1 & -1 \\ 0 & 0 & 0 & 0 & 0 & 1 & -1 & -1 & 1 \\ 0 & 0 & 0 & 0 & 0 & 1 & -1 & 1 & -1 \\ 0 & 0 & 0 & 0 & 0 & 1 & 1 & 1 & 1 \end{bmatrix}. \quad (32)$$

The T matrix ($T = NM$) is rewritten $N = TM^{-1}$:

$$N = \begin{bmatrix} 1 & 0 & 0 & 0 & 0 & 0 & 0 & 0 & 0 \\ -u_x & 1 & 0 & 0 & 0 & 0 & 0 & 0 & 0 \\ -u_y & 0 & 1 & 0 & 0 & 0 & 0 & 0 & 0 \\ u_x^2 + u_y^2 & -2u_x & -2u_y & 1 & 0 & 0 & 0 & 0 & 0 \\ u_x^2 - u_y^2 & -2u_x & 2u_y & 0 & 1 & 0 & 0 & 0 & 0 \\ u_x u_y & -u_y & -u_x & 0 & 0 & 1 & 0 & 0 & 0 \\ -u_x^2 u_y & 2u_x u_y & u_x^2 & -u_y/2 & -u_y/2 & -2u_x & 1 & 0 & 0 \\ -u_x u_y^2 & u_y^2 & 2u_x u_y & -u_x/2 & u_x/2 & -2u_y & 0 & 1 & 0 \\ u_x^2 u_y^2 & -2u_x u_y^2 & -2u_x^2 u_y & (u_x^2 + u_y^2)/2 & -(u_x^2 - u_y^2)/2 & 4u_x u_y & -2u_y & -2u_x & 1 \end{bmatrix}, \quad (33)$$

where $\Lambda = M^{-1} N^{-1} K N M$. Top boundary of lattice Boltzmann equation is:

$$f_4 = f_2, \quad f_7 = f_5 + \frac{1}{2}(f_1 - f_3) + \frac{1}{4}(F_x + F_y), \quad (34)$$

$$f_8 = f_6 - \frac{1}{2}(f_1 - f_3) - \frac{1}{4}(F_x - F_y). \quad (35)$$

Bottom boundary of lattice Boltzmann equation is:

$$f_2 = f_4, \quad f_5 = f_7 - \frac{1}{2}(f_1 - f_3) - \frac{1}{4}(F_x + F_y), \quad (36)$$

$$f_6 = f_8 + \frac{1}{2}(f_1 - f_3) + \frac{1}{4}(F_x - F_y). \quad (37)$$

Left boundary of lattice Boltzmann equation is:

$$f_1 = f_3, \quad f_5 = f_7 - \frac{1}{2}(f_2 - f_4) - \frac{1}{4}(F_x + F_y), \quad (38)$$

$$f_8 = f_6 + \frac{1}{2}(f_2 - f_4) + \frac{1}{4}(-F_x + F_y). \quad (39)$$

Right boundary of lattice Boltzmann equation is:

$$f_3 = f_1, \quad f_7 = f_5 + \frac{1}{2}(f_2 - f_4) + \frac{1}{4}(F_x + F_y), \quad (40)$$

$$f_6 = f_8 - \frac{1}{2}(f_2 - f_4) - \frac{1}{4}(-F_x + F_y). \quad (41)$$

Thermal boundary condition is

$$\begin{cases} g_2(i,j) = T_w \cdot (\omega(4) + \omega(2)) - g_4(i,j+1) \\ g_5(i,j) = T_w \cdot (\omega(7) + \omega(5)) - g_7(i,j+1) \\ g_6(i,j) = T_w \cdot (\omega(8) + \omega(6)) - g_8(i,j+1) \end{cases} \quad (42)$$

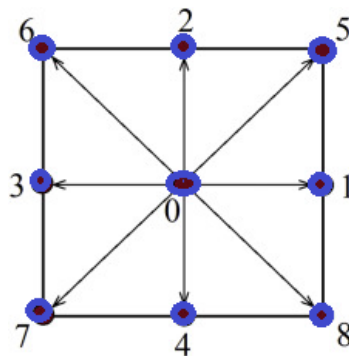


Figure 2. LBM 2D lattice.

4. Results

In this section, the results of numerical investigations are presented. The maximum velocity for different interfacial thickness ζ in Equation (2), or the velocity errors as a function of the number of lattices could be used as validation. For the case of verifications, the Nusselt number was studied in Table 2. The cross-section Boltzmann technique is a liquid numerical reenactment strategy produced throughout the previous thirty years. Applied in numerous zones, which might be hard for customary strategies, for example, miniaturized scale stream and warmth move, permeable media, attractive liquid, and so forth. The cross-section Boltzmann technique has the benefits of intrinsic parallelism, just as basic limit condition handling and simple usage of the program. Magnetic field Norm normal to magnet direction is shown in Figure 3.

Table 2. Grid study.

Grid Number	60 × 60	80 × 80	100 × 100	120 × 120
Nu	2.113	2.0511	2.032	2.01

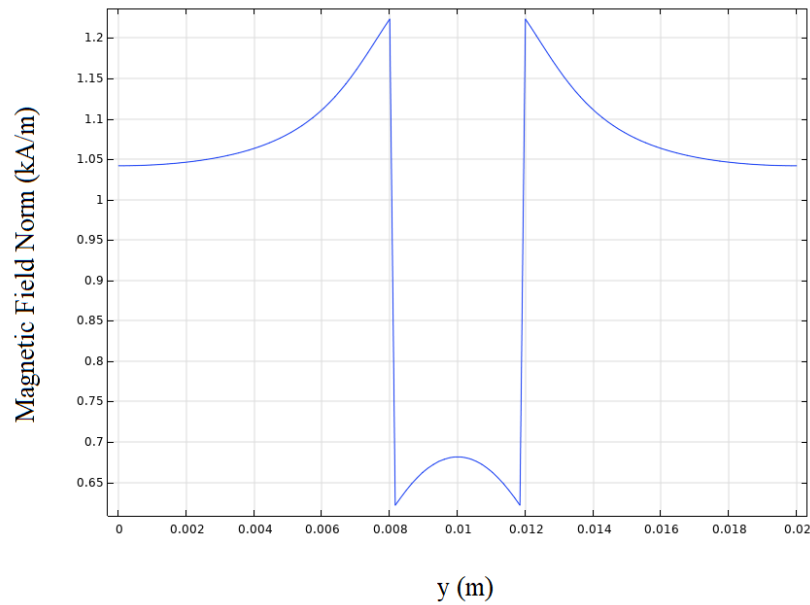
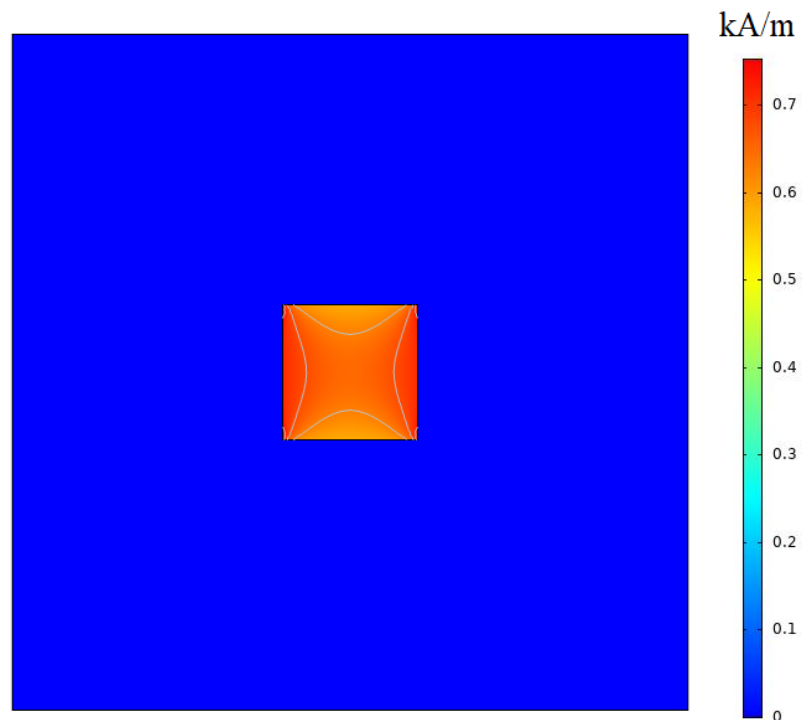
**Figure 3.** Magnetic field Norm normal to magnet direction.

Figure 4 shows the Magnetization Vector. To check the accuracy and count of characteristic convection, and the outcomes were contrasted and information provided by other researchers. As appeared in Figure 4, the count methodology is adequately precise.

**Figure 4.** Magnetization Vector.

To check the impact of matrix numbers on the recreated arrangement, the mimicked heat move execution under various network numbers has appeared in Table 1, for the $Ra = 4 \times 10^4$. A Nusselt number value from 80×80 grid changes nearly nothing. Thinking about the exactness and computational intricacy, the number of frameworks is considered by 100×100 .

Figure 5 presents the Magnetic field Norm. To examine the impact of the straight move in the depression, a thermal field examination of the pit by a direct cathode appear in the next Table 2 and figure, individually. As seen in Table 2, contrasted with the no boundary condition, the warmth move execution with liner cathode is marginally debilitated, not over 3 percent. The temperature profile in Figure 5 additionally shows that the impact of the straight cathode on the general temperature field dispersion is moderately small and might be immaterial.

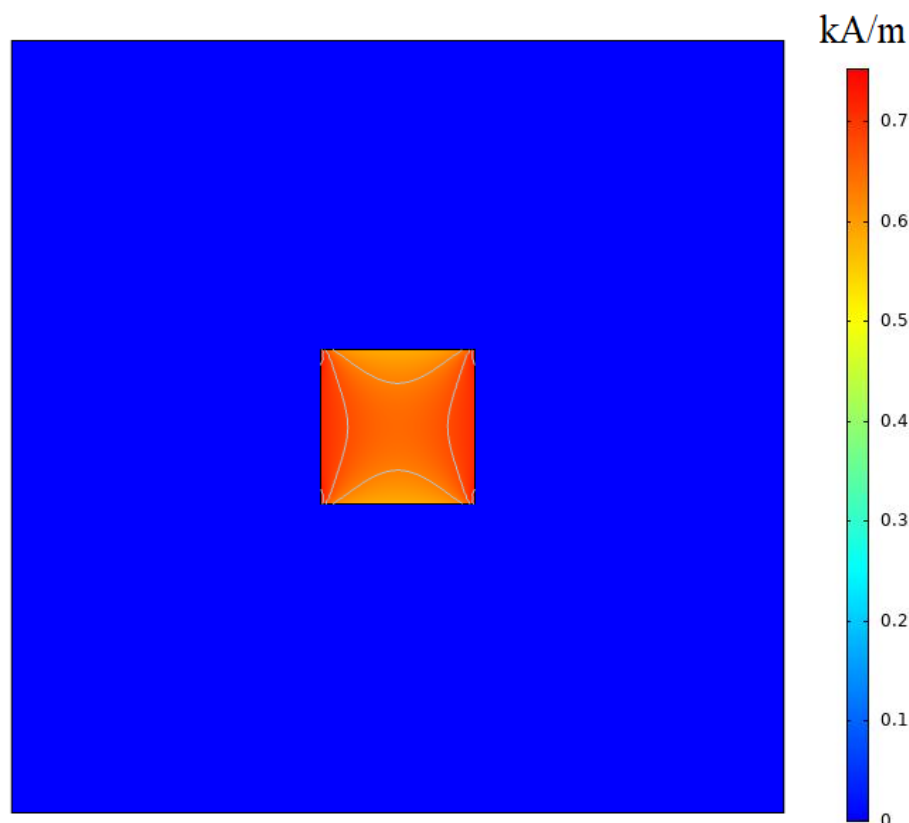


Figure 5. Magnetic field Norm.

Figure 6 reveals the Magnetic Flux Density Norm. Right off the magnetic element, the impact of the applied magnetic field move qualities of the liquid is mimicked under the states of the top warming and the base at a steady-state gravity field. Figure 6 presents the correlation of the test and reproduction of the Magnetic Flux Density Norm of the proportion of warmth move by a Magnetic field. Without gravity, relates to unadulterated warm conduction. It very well may be concluded from Figure 6 that an arrangement of warmth move with a decent concurrence with the trial esteems at various warmth transitions, which affirms great exactness of the magnetic power. As shown in Figure 6, heat move upgrade proportion increases as voltage and warmth motion increase. Plus, as the voltage builds, the heat move improvement proportion expands increasingly quickly. In the test run, the heat move coefficient can be improved on multiple occasions, contrasted with unadulterated conduction.

Figure 7 shows Magnetic Flux Density Vector. Figure 7 is a correlation speed at various magnetic and flatways on the middle vertical segment within the domain. As the liquid is static it has not affected the magnetic field. At the point when the magnetic field concentrates near the heater corner, the impact of the electric field on the magnetic field is as yet immaterial. Be that as it may, when

the magnetic value increases, the conspicuous impact happens and the oil starts to stream. Near the middle, the more noteworthy the fluid motion.

Flux Density Norm (mf).png

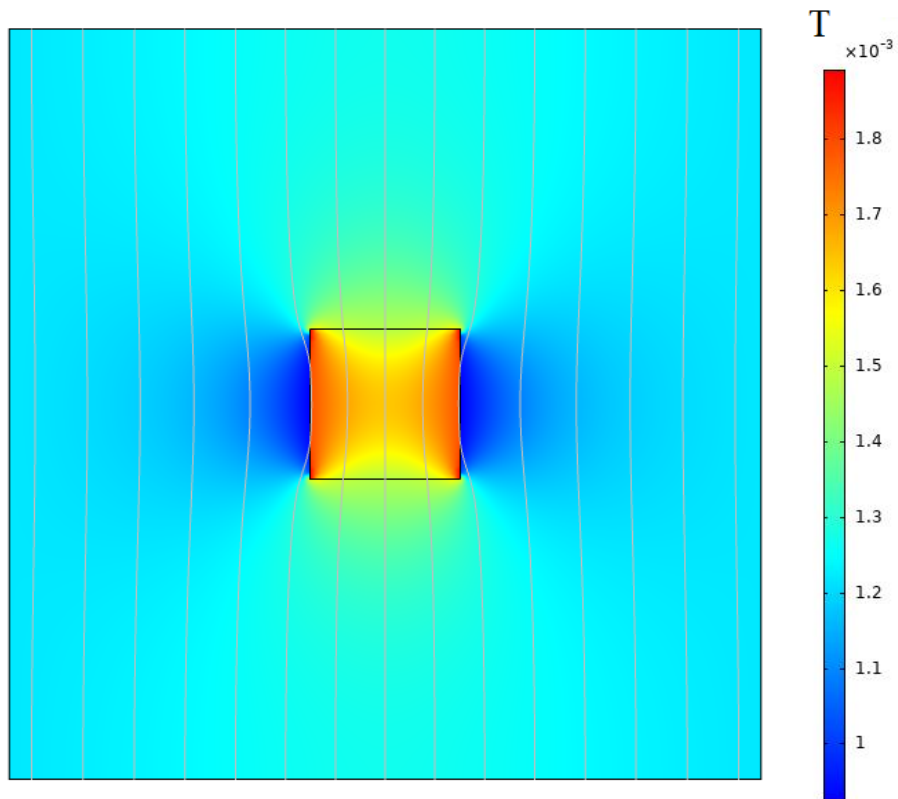


Figure 6. Magnetic Flux Density Norm.

Flux Density Vector (B).png

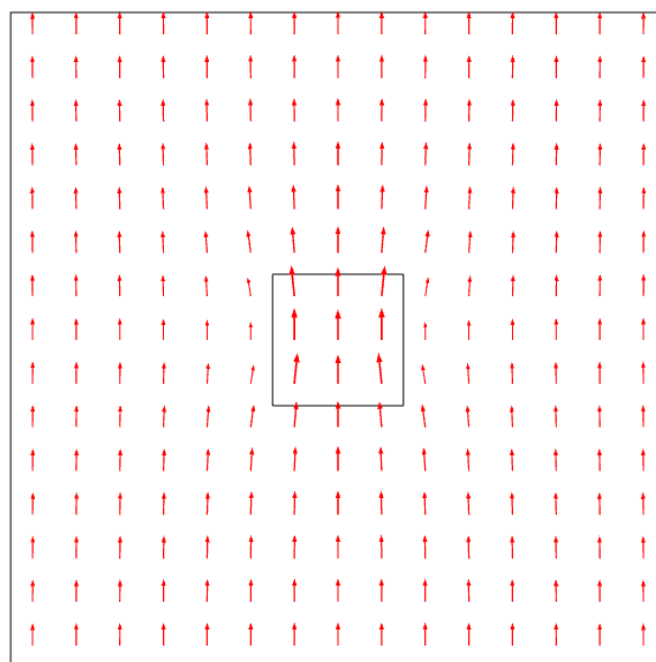


Figure 7. Magnetic Flux Density Vector.

Figure 8 shows that the Magnetization Norm Charge—also named attractive polarization—is a vector amount that gives the proportion of the thickness of perpetual or prompted dipole second in a given attractive material.

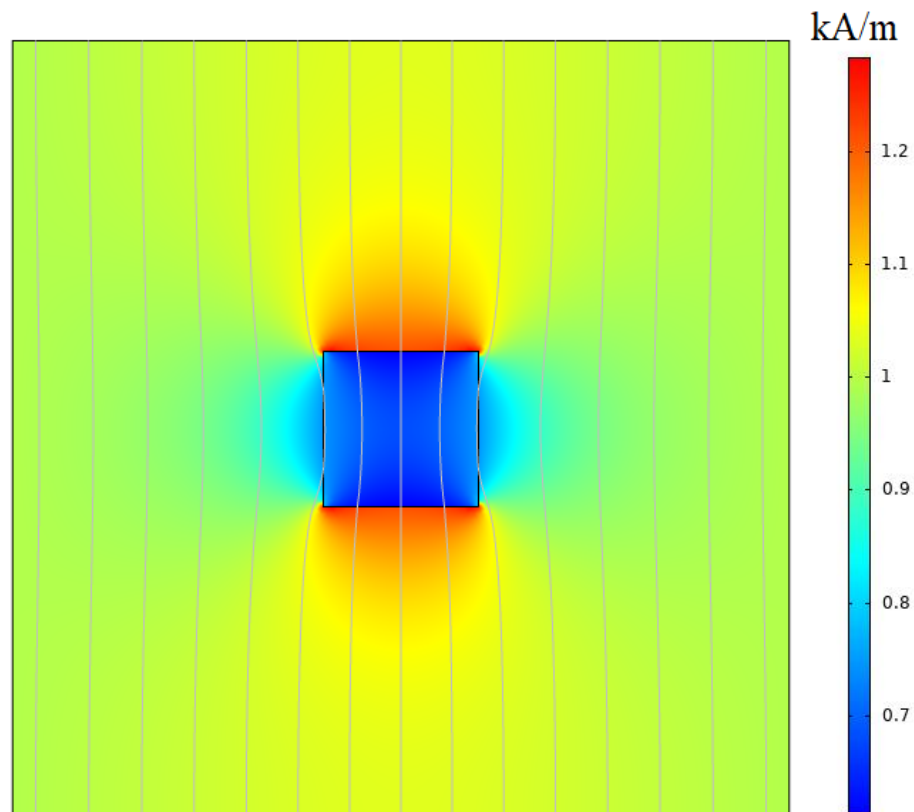


Figure 8. Magnetization Norm.

Figure 9 presents the Bubble growth profiles. Air pocket development inside a superheated fluid drop will be viewed first. That cooling continues gradually as the warm profile in the polymer fluid alters. At the point when the magnet's leftover motion thickness (magnetic flux) is 0.1 T or 0.2 T, the attractive power has no huge impact on the air pocket shape; when this thickness is 0.3 T, the fume layer is somewhat more slender, and when it is 0.4 T, the principal bubble flight happens as of now. Expanding the magnetic flux to 0.5 T further quickens the air pocket age process, which for this situation, has brought about the takeoff of a subsequent air pocket.

Figure 10 presents the magnitude of the effect of the magnetic field on the average Nusselt number. It seems that by augmentation of the magnetic field strength, the fluid forces around the square increase. It also causes separation of bubble from the surface sooner. This behavior lessens the boundary layer thickness and increases the heat flux from the surface.

Figure 11 presents the magnetic field angle effects on the average Nusselt number. It seems that by augmentation of the magnetic field strength the fluid forces around the square change its direction. It also causes complex separation of bubbles from the surface. This behavior changes the boundary layer thickness in all directions and increases the heat flux from the surface but it depends on the angle.

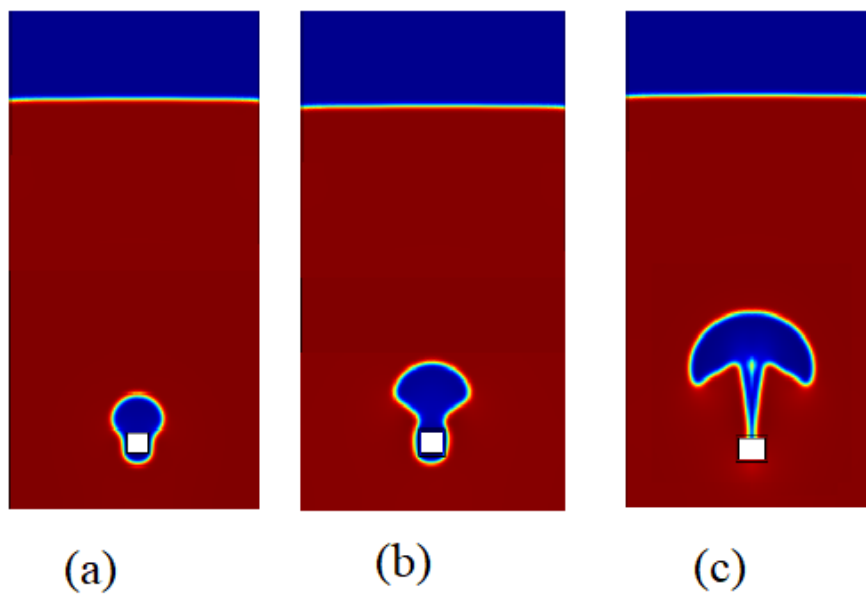


Figure 9. Bubble growth profiles.

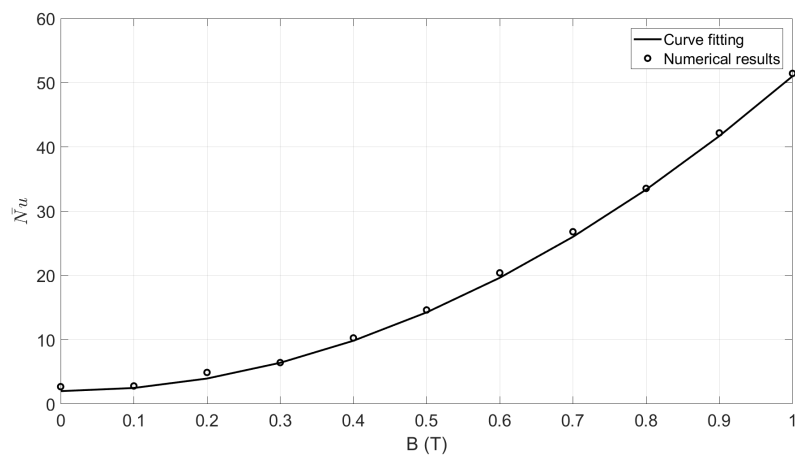


Figure 10. Effect of magnetic field magnitude on average Nusselt number.

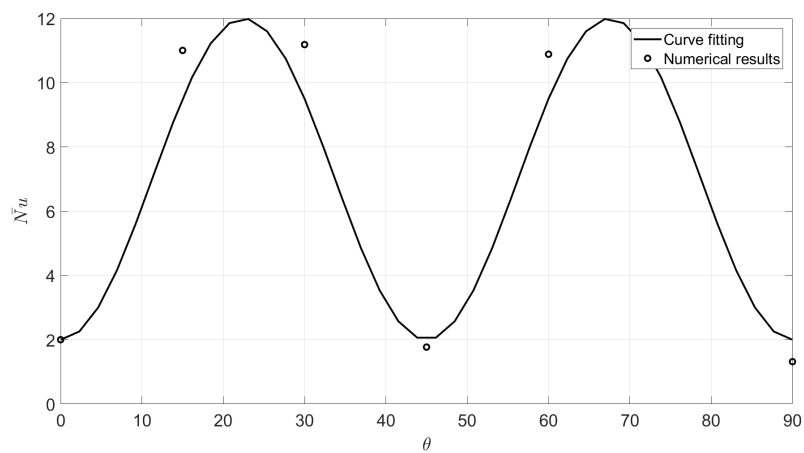


Figure 11. Effect of magnetic field angle on average Nusselt number.

Finally, the effect of magnetic field magnitude and angle on the value of the Nusselt number is estimated by:

$$Nu(\theta, t) = 2 + 49B^2 + 10\sin\left(\frac{4\theta}{\pi}\right)^2. \quad (43)$$

Velocity vectors in bubble growth in a vertical arrangement are presented in Figure 12. This is on the grounds that, as the lightness power pushes the fume bubble upward, the attractive power pulls the MNF down, which forestalls the arrangement of a fume segment as when the magnetic flux is 0.1 T. One can watch very thin fume layers on numerous pieces of the chamber surface, which implies an improvement in the warmth move in light of the diminished superheating temperature distinction. As the attractive power applied to the interface builds, it begins to sabotage the film bubbling insecurity and crack the fume layers on certain pieces of the chamber. More grounded attractive powers can balance out the circumstance and block the film bubbling procedure.

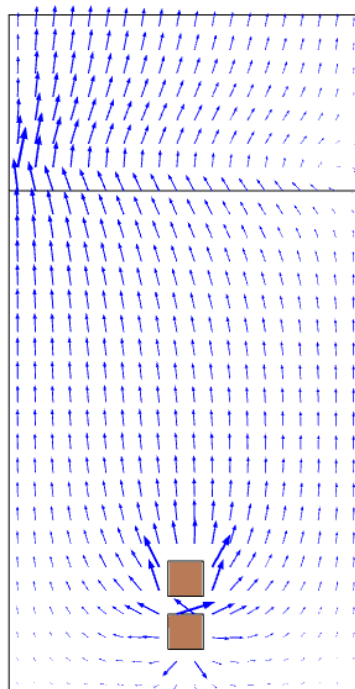


Figure 12. Velocity vectors in bubble growth in vertical arrangement.

Figure 13 shows the vapour motion in a vertical arrangement. This is in light of the fact that as the delicacy power growth of bubble in a vertical direction, the appealing force fluid dropping, which hinders the course of action of a vapour section as when the magnetic flux is 0.1 T. Slim vapour layers on various bits of the chamber suggest an improvement in the glow move considering the reduced superheat temperature differentiation. As the alluring bubble fabricates, it starts to disrupt the film foaming uncertainty and break the bubble on specific bits of the chamber. More grounded alluring forces can adjust the condition and square the film gurgling methodology.

Figure 14 shows the Bubble growth in a horizontal arrangement. As this plot outlines, there is not a lot of contrast for the heat transfer rate for low magnetic flux values, which implies the attractive field does not influence the pace of warmth move at the chamber surface. Be that as it may, the heat transfer by convection is where particular pinnacles and valleys mirror the occasional flight of fume bubbles. At higher magnetic flux values, the Nusselt numbers are drastically higher in light of the fact that the attractive field is solid to the point that the fume vapour chamber turns out to be very slender.

Figure 15 shows the magnetic field angle effect on Bubble growth. Figure 15 shows the air pocket development beginning time in the recreations with various θ values. When the force is horizontal, the fume film around the heater is significantly thick. In any case, when $\theta = 20$, the fume film at the highest point of the chamber is extremely slight, because of the thicker boundary layer a higher warmth move rate happens. At the point when the post direction is at $\theta = 20$, the fume layer is scattered all around the chamber. At $\theta = 20$, the movement of the air pockets is arbitrary and scattered and bubble takeoff is not, at this point occasional. At $\theta = 20$, for example, at the point when the shafts are flawlessly vertical, the fume layer is altogether higher on the base of the chamber.

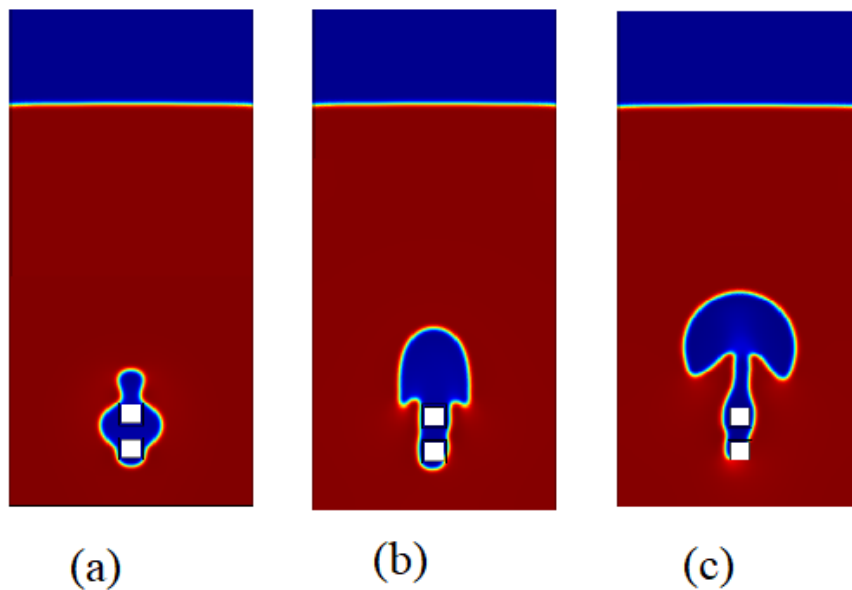


Figure 13. Bubble growth in vertical arrangement.

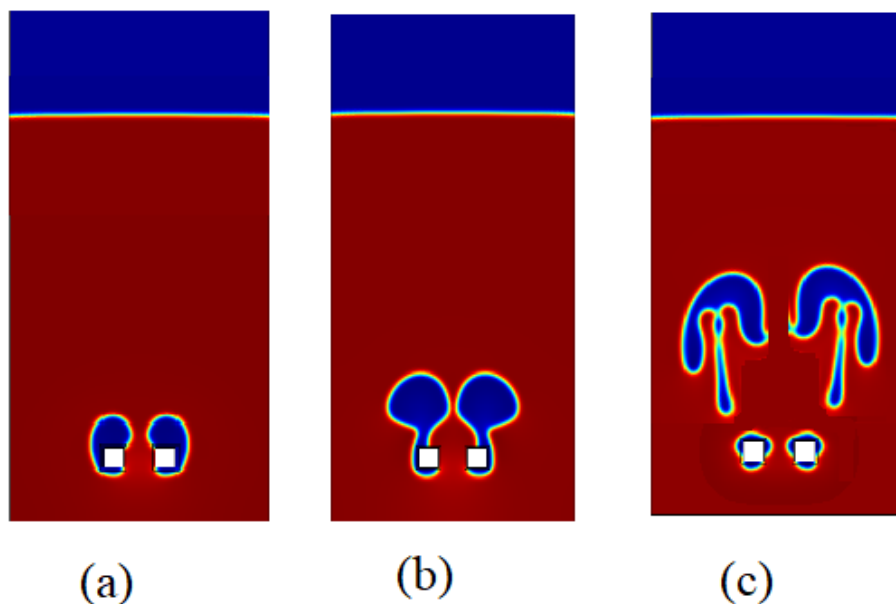


Figure 14. Bubble growth in horizontal arrangement.

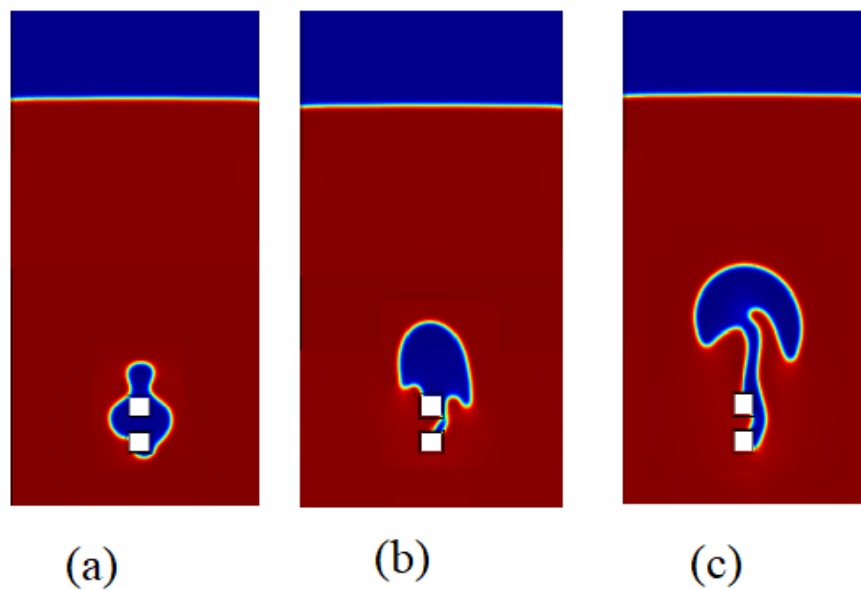


Figure 15. Effect of magnetic field angle on Bubble growth.

5. Conclusions

In this paper, two-phase film boiling of ferrofluids under an external magnetic field was performed around a square cross-section heater. The central-moments-based lattice Boltzmann method was used to solve the governing mass, momentum, and energy equations. The following results are obtained:

- (1) By the increase of magnitude magnetic flux, the heat transfer increased.
- (2) By the increase of angle of application of magnetic flux, the heat transfer increased. The increase is a function of the magnet angle.
- (3) A correlation to obtain the Nusselt number was presented.

The study presented a novel method to analyze film boiling in two-dimensional geometries. The geometry of the square heater was studied where not enough attention has been paid to this in previous literature. It is proposed to extend this study for other geometries such as triangle and rectangular heaters. Other ferrofluids and optimized magnetic fields can also be used to obtain the best heat transfer rates. In the typical film boiling system considered, the fluid temperature is initially near saturation temperature and after phase change it leaves the heater boundary. Because of the nature of phase change, the system remains near the saturation temperature. The dimensionless temperature ratio, $\frac{T - T_{sat}}{T_w - T_{sat}}$, is near zero. For finding the precise effect of temperature on the system properties, further investigations are recommended.

Funding: This research received no external funding.

Conflicts of Interest: The authors declare no conflict of interest.

Nomenclature

C_p	specific heat capacity (J/kg K)
g	acceleration due to gravity (m/s^2)
h	heat transfer coefficient ($W/(m^2 K)$)
h_{fg}	latent heat (J/kg)
k	thermal conductivity ($W/m K$)
L	characteristic length (m)
Nu	local Nusselt number
Nu_m	mean Nusselt number for whole heater surface
P	Pressure (N/m^2)

Pr	Prandtl number
q''	Heat flux (W/m^2)
Ra	Rayleigh number
t	Time (s)
T	temperature (K)
u	vapour velocity in x-direction (m/s)
v	velocity normal to the direction of flow (m/s)
x	horizontal coordinate (m)
y	coordinate measured distance normal to heater surface (m)

Greek symbols

α	Void fraction
δ	vapour film thickness (m)
μ	absolute viscosity (kg/ms)
ν	kinematic viscosity (m^2/s)
ρ	density (kg/m^3)
θ	angle measured from horizontal of heater; Azimuthal angle (rad or degrees) angle of inclination with respect to the horizontal plane

Subscripts

eq	Equilibrium
f	Saturated liquid
FB	Film boiling
l	liquid
m	Mixture, mixture average
NB	Nucleate boiling
ref	Reference
s	vapour at saturation temperature
sat	Saturation
v	vapour
w	heater wall
∞	Ambient associated with a large surface

References

- Sedaghatkish, A.; Sadeghiseraji, J.; Jamalabadi, M.Y.A. Numerical simulation of magnetic nanofluid (MNF) film boiling on cylindrical heated magnet using phase field method. *Int. J. Heat Mass Transf.* **2020**, *152*, 119546. [[CrossRef](#)]
- Liang, G.; Mudawar, I. Review of pool boiling enhancement by surface modification. *Int. J. Heat Mass Transf.* **2019**, *128*, 892–933. [[CrossRef](#)]
- Kandlikar, S.G. Fundamental issues related to flow boiling in minichannels and microchannels. *Exp. Therm. Fluid Sci.* **2002**, *26*, 389–407. [[CrossRef](#)]
- Kandlikar, S.G.; Balasubramanian, P. An extension of the flow boiling correlation to transition, laminar, and deep laminar flows in minichannels and microchannels. *Heat Transf. Eng.* **2004**, *25*, 86–93 [[CrossRef](#)]
- Shojaeian, M.; Koşar, A. Pool boiling and flow boiling on micro- and nanostructured surfaces. *Exp. Therm. Fluid Sci.* **2015**, *63*, 45–73. [[CrossRef](#)]
- Phan, H.T.; Caney, N.; Marty, P.; Colasson, S.; Gavillet, J. Surface wettability control by nanocoating: The effects on pool boiling heat transfer and nucleation mechanism. *Int. J. Heat Mass Transf.* **2009**, *52*, 5459–5471. [[CrossRef](#)]
- Liter, S.G.; Kaviany, M. Pool-boiling CHF enhancement by modulated porous-layer coating: Theory and experiment. *Int. J. Heat Mass Transf.* **2001**, *44*, 4287–4311. [[CrossRef](#)]
- Liang, G.; Mudawar, I. Review of pool boiling enhancement with additives and nanofluids. *Int. J. Heat Mass Transf.* **2018**, *124*, 423–453. [[CrossRef](#)]
- Abe, Y. Self-wetting fluids: Beneficial aqueous solutions. *Ann. N. Y. Acad. Sci.* **2006**, *1077*, 650–667. [[CrossRef](#)]
- Wang, L.; Yue, X.; Chong, D.; Chen, W.; Yan, J. Experimental investigation on the phenomenon of steam condensation induced water hammer in a horizontal pipe. *Exp. Therm. Fluid Sci.* **2018**, *91*, 451–458. [[CrossRef](#)]

11. Levin, A.A.; Tairov, E.A.; Spiryaev, V.A. Self-excited pressure pulsations in ethanol under heater subcooling. *Thermophys. Aeromech.* **2017**, *24*, 61–71. [[CrossRef](#)]
12. Clough, R.W.; Penzien, J. *Dynamics of Structures*; McGraw-Hill Book Company: New York City, NY, USA, 1975; Volume 3, pp. 310–311.
13. Ivey, H.J.; Morris, D.J. *Critical Heat Flux of Saturation and Subcooled Pool Boiling in Water at Atmospheric Pressure*; Begel House Inc.: Danbury, CT, USA, 1966; Volume 9, pp. 129–1420.
14. Zuber, N. Hydrodynamic Aspect of Boiling Heat Transfer. Ph.D. Thesis, University of California, Los Angeles, CA, USA, 1959.
15. Kutateladze, S.S. *Heat Transfer in Condensation and Boiling*; AEC-Transl.: Washington, DC, USA, 1952; Volume 5, pp. 3700–3770.
16. Inada, S.; Miyasaka, Y.; Sakamoto, S.; Chandratilleke, G.R. Liquid-solid contact state in subcooled pool transition boiling system. *J. Heat Transf.* **1986**, *108*, 219–221. [[CrossRef](#)]
17. Unno, N.; Yuki, K.; Kibushi, R.; Suzuki, K. Advanced boiling cooling technology using a compact vessel with a low water level. *Trans. Jpn. Inst. Electron. Packag.* **2018**, *11*, E18-010. [[CrossRef](#)]
18. Sjölander, K.; Beskow, J. Wavesurfer—an open source speech tool. In Proceedings of the Sixth International Conference on Spoken Language Processing, Beijing, China, 16–20 October 2000.
19. Katto, Y.; Yokoya, S.; Teraoka, K. Experimental study of nucleate boiling in case of making interference-plate approach to the heating surface. In Proceedings of the 3th International Heat Transfer Conference, Chicago, IL, USA, 7–12 August 1966; Volume 3, pp. 219–227.
20. Zhao, Y.; Tsuruta, T.; Ji, C. Experimental study of nucleate boiling heat transfer enhancement in a confined space. *Exp. Therm. Fluid Sci.* **2003**, *28*, 9–16. [[CrossRef](#)]
21. Fakhari, A.; Bolster, D. Diffuse interface modeling of three-phase contact line dynamics on curved boundaries: A lattice Boltzmann model for large density and viscosity ratios. *J. Comput. Phys.* **2017**, *334*, 620–638. [[CrossRef](#)]
22. Abdollahzadeh Jamalabadi, M.Y. LBM simulation of piezo fan in square enclosure. *Int. J. Numer. Methods Heat Fluid Flow* **2019**, *30*, 401–426. [[CrossRef](#)]
23. Sadeghi, R.; Shadloo, M.S.; Jamalabadi, M.Y.A.; Karimipour, A. A three-dimensional lattice Boltzmann model for numerical investigation of bubble growth in pool boiling. *Int. Commun. Heat Mass Transf.* **2016**, *79*, 58–66. [[CrossRef](#)]
24. de Rosis, A.; Huang, R.; Coreixas, C. Universal formulation of central-moments-based lattice Boltzmann method with external forcing for the simulation of multiphysics phenomena. *Phys. Fluids* **2019**, *31*, 117102. [[CrossRef](#)]
25. Saito, S.; de Rosis, A.; Fei, L.; Luo, K.H.; Ebihara, K.; Kaneko, A.; Abe, Y.; Koyama, K. Lattice Boltzmann modeling and simulation of forced-convection boiling on a cylinder. *arXiv* **2019**, arXiv:1912.02018
26. Saito, S.; De Rosis, A.; Festuccia, A.; Kaneko, A.; Abe, Y.; Koyama, K. Color-gradient lattice Boltzmann model with nonorthogonal central moments: Hydrodynamic melt-jet breakup simulations. *Phys. Rev. E* **2018**, *98*, 013305. [[CrossRef](#)]
27. Saito, S.; Abe, Y.; Koyama, K. Lattice Boltzmann modeling and simulation of liquid jet breakup. *Phys. Rev. E* **2017**, *96*, 013317. [[CrossRef](#)] [[PubMed](#)]
28. De Rosis, A. Central-moments-based lattice Boltzmann schemes with force-enriched equilibria. *EPL (Europhys. Lett.)* **2017**, *117*, 34003. [[CrossRef](#)]
29. De Rosis, A. Non-orthogonal central moments relaxing to a discrete equilibrium: A D2Q9 lattice Boltzmann model. *EPL (Europhys. Lett.)* **2016**, *116*, 44003. [[CrossRef](#)]
30. Krakov, M.S.; Nikiforov, I.V. Natural convection in a horizontal cylindrical enclosure filled with a magnetic nanofluid: Influence of the uniform outer magnetic field. *Int. J. Therm. Sci.* **2018**, *133*, 41–54. [[CrossRef](#)]
31. Krakov, M.S.; Nikiforov, I.V. Influence of the shape of the inner boundary on thermomagnetic convection in the annulus between horizontal cylinders: Heat transfer enhancement. *Int. J. Therm. Sci.* **2020**, *153*, 106374. [[CrossRef](#)]

